# Reply to Editor

We appreciate your consideration for improving the manuscript.

Following your suggestion, we conduct two additional experiments that are 1) the tracer advection over the mountain of Schär et al. which has 3km maximum height (see eq.(26a) and (26b) in Schär et al. (2002)) and 2) the Schär mountain gravity wave. The mountain profiles and background settings are identical to Schär et al. (2002).

a. the tracer advection over the mountain

For this experiment, the 2DNH is initialized using the same initial conditions and mountain profile in Schär et al. (2002) (hereafter, SC02) and we analyze our results using the same format of figures of SC02.

The mountain profile is given by eq.(26a and 26b) in SC02, the prescribe wind profile is equivalent to eq.(28) in SC02, and initial tracer is assigned with eq.(30) in SC02. A more detailed description of the profiles can be found in SC02.

The advection equation for tracer $q$ which we consider in 2D frame is

$$\frac{\partial q}{\partial t} = -(u\frac{\partial q}{\partial x} + \dot{\eta}\frac{\partial q}{\partial \eta}) .$$

The domain is defined as $(x,z) \in [-150,150] \times [0,25]$ km$^2$. The model is integrated with a grid resolution of $\Delta\overline{x} = 300$ m using 5th order basis polynomials per element and $\Delta\overline{z} = 250$ m using 100 levels for 5000s without any diffusion, filter, and limiter.

The numerical solutions and the error field are shown in Auxiliary Fig. 1. Even at t=2500s at which the center of the tracer locates over the center of the mountain, the distribution of the initial tracer is generally maintained (Aux. Fig.1a). It means that the 2DNH using horizontally spectral element vertically finite difference method can produce numerical solutions of good quality in response to the strong vertical gradient in the coordinate deformation. It is noteworthy that in Aux. Fig.1b the error at t=5000s give ranges of $\left[-2.71\times10^{-2}, 2.35\times10^{-2}\right]$ which is substantially small, and the error is distributed mainly over the mountain where the distortion of the computational grid is significant.

b. Schär mountain gravity wave

The initial conditions and mountain profile are the same as SC02 (the Brunt-Väisälä frequency of $N = 0.01$ /s, the constant mean flow of $\bar{U} = 10$ m/s, the initial temperature of $T_0 = 288$ K). The domain is defined as $(x, z) \in [-30, 30] \times [0, 21]$ km$^2$. The model is integrated with a grid resolution of $\Delta\bar{x} = 300$ m using 5th order basis polynomials per element and $\Delta\bar{z} = 250$ m using 80 levels for 10-hour without any diffusion or viscosity. The bottom boundary uses a no-flux boundary condition while the lateral and top boundaries use sponge layers. The sponged zone is 10 km deep from the top and 5 km wide from the lateral boundaries. Over the sponge layer zone, the prognostic variables are relaxed to the initial state.

Auxiliary Fig. 2 shows the simulated results of perturbed horizontal and vertical wind speeds after 10 h. In comparison with its analytic solution, the numerical solutions match the analytic solution quite well. Also in comparison with the results of other numerical models (Giraldo and Restelli 2008; Li et al 2013), the results of the present model look very similar. For quantitative comparison, we present the root-mean-square errors for $u'$, $w'$, and $\theta'$ in Auxiliary Table 1. These numbers are competitive to those of other numerical models (Giraldo and Restelli 2008; Li et al 2013).

# References

Giraldo, F. X. and M. Restelli, 2008: A study of spectral element and discontinuous Galerkin methods for the Navier-Stokes equations in nonhydrostatic mesoscale atmospheric modeling: equation sets and test cases. Journal of computational physics 227, 3849-3877.

Li, X., C. Chen, X. Shen, and F. Xiao, 2013: A multimoment constrained finite-volume model for nonhydrostatic atmospheric dynamics. Mon. Wea. Rev., 141, 1216-1240.

Schär, C., D. Leuenberger, O. Fuhrer, D. Lüthi, and C. Girard, 2002: A new terrain-following vertical coordinate formulation for atmospheric prediction models. Mon. Wea. Rev., 130, 2459-2480.

Auxiliary Table 1. Root-mean-square errors of the Schär mountain after 10-hour for $\Delta\overline{x} = 300$ m using the 5th order polynomials per elements and $\Delta\overline{z} = 250$ m using 80 levels.

| Variable | RMSE |
|---|---|
| $u$ (m s$^{-1}$) | $1.43 \times 10^{-1}$ |
| $w$ (m s$^{-1}$) | $3.97 \times 10^{-2}$ |
| $\theta$ (K) | $3.77 \times 10^{-2}$ |

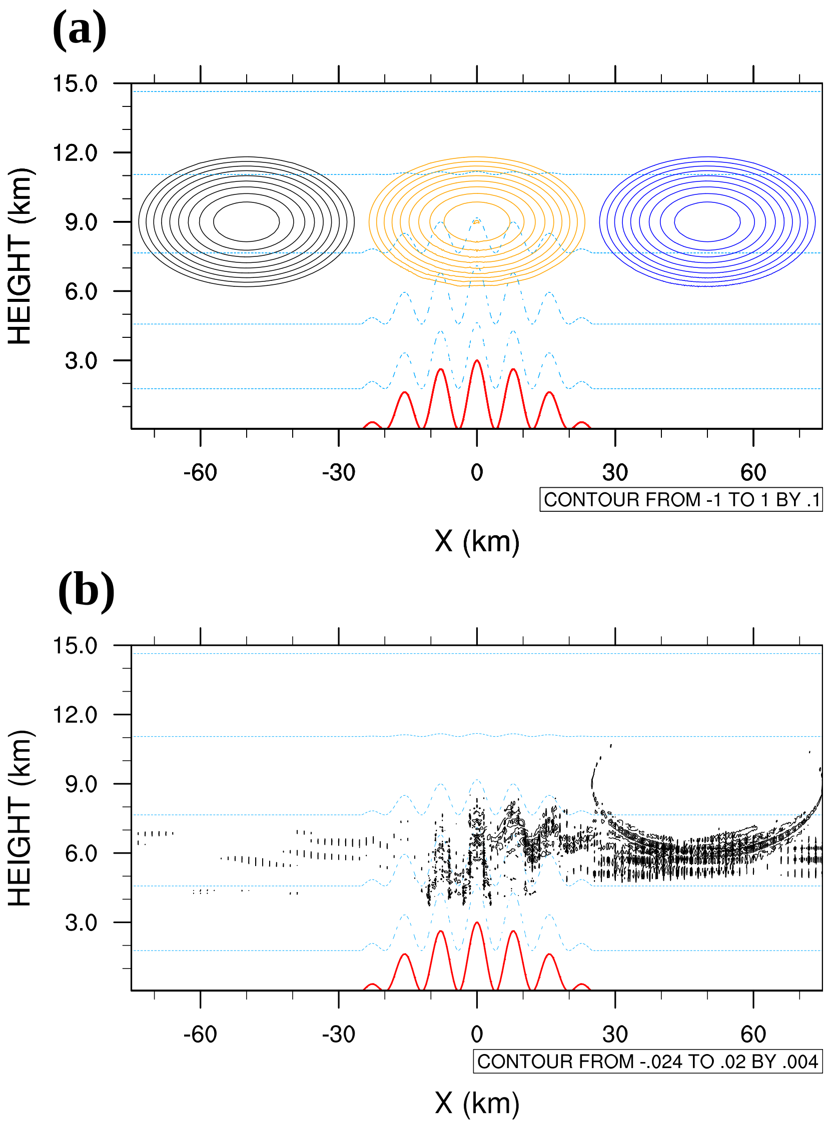


Auxiliary FIG. 1. The tracer advection test over the topography (red line) of Schär et al. (see eq.(26a) and (26b) in Schär et al. (2002)). (a) the advective tracer at time 0 (black line), 2500s (orange), and 5000s (blue), and (b) the error at time 5000s. The numerical solutions are obtained with a grid resolution of $\Delta\overline{X} = 300$ m using 5th order basis polynomials per element and $\Delta\overline{Z} = 250$ m. The sky blue dash lines indicate the surfaces of constant eta. The zero contour level is omitted.

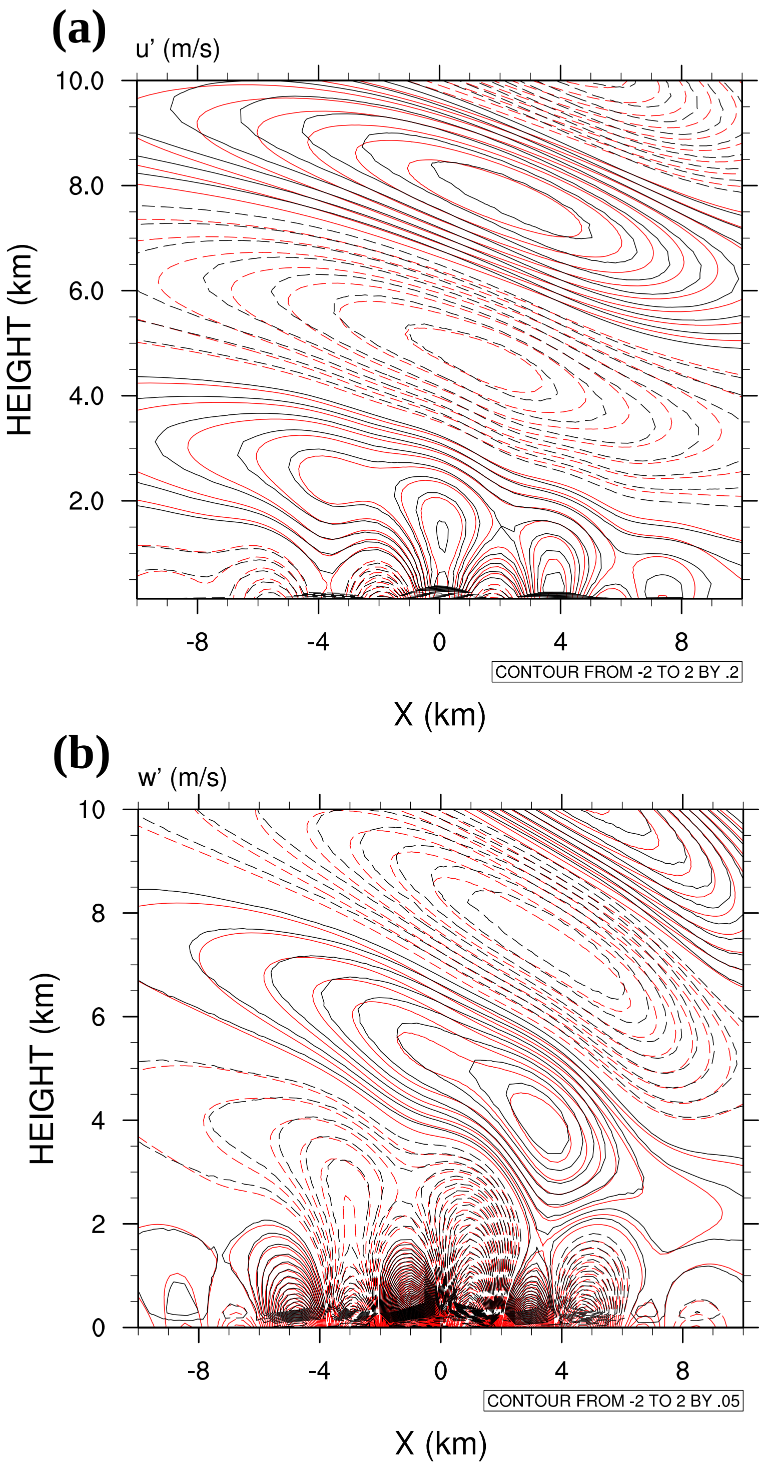


Auxiliary FIG. 2. Steady-state flow of (a) perturbed horizontal velocity (m/s) and (b) vertical velocity (m/s) over the Schär Mountain after 10-hour with a grid resolution of $\Delta\overline{x} = 300$ m using 5th order basis polynomials per element and $\Delta\overline{z} = 250$ m. The numerical solution is represented by black lines and the analytic solution by led lines. Dashed lines denote negative values.